CHEMISTRY OF MATERIALS

Bending Type Electron Donor-Donor-Acceptor Triad: Dual Excited-State Charge-Transfer Coupled Structural Relaxation

Jia-An Lin, Shu-Wei Li, Zong-Ying Liu, Deng-Gao Chen, Chun-Ying Huang, Yu-Chen Wei, Yi-Yun Chen, Zheng-Hua Tsai, Chun-Yuan Lo, Wen-Yi Hung, Ken-Tsung Wong, and Pi-Tai Chou

Just Accepted

Bending Type Electron Donor-Donor-Acceptor Triad: Dual Excited-State Charge-Transfer Coupled Structural Relaxation

Jia-An Lin,[†] Shu-Wei Li,[†] Zong-Ying Liu,[†] Deng-Gao Chen,[†] Chun-Ying Huang,[†] Yu-Chen Wei,[†] Yi-Yun Chen,[†] Zheng-Hua Tsai,[‡] Chun-Yuan Lo,[†] Wen-Yi Hung,*,[‡] Ken-Tsung Wong,*,[†,#] Pi-Tai Chou,*,[†]

[†] Department of Chemistry, National Taiwan University, Taipei, 10617 Taiwan

[‡] Institute of Optoelectronic Sciences, National Taiwan Ocean University, Keelung, 20224, Taiwan

[#] Institute of Atomic and Molecular Science, Academia Sinica, Taipei, 10617 Taiwan

*e-mail: wenhung@mail.ntou.edu.tw; kenwong@ntu.edu.tw; chop@ntu.edu.tw

[⊥] J.-A. L., S.-W. L. and Z.-Y. L. made equal contributions.

ABSTRACT: The triad types of molecules with various combinations of electron donor (D) and acceptor (A) have been widely exploited in optoelectronics. However, their photophysical and photochemical properties, which are frequently unconventional, are relatively unexplored. In this study, a donor-donor-acceptor (D-D-A) type triad, **CTPS**, consisting of the donor moiety of triphenylamine (D1) and the acceptor moiety of dibenzothiophene sulfone (A) bridging through the second donor carbazole (D2) into a U-shape configuration, was synthesized. **CTPS** exhibited dual emission bands, both of which reveal solvent polarity dependent solvatochromism and unusual excitation-wavelength dependent ratiometric emission. Comprehensive studies clarified that two emissions originate from two different D-A charge transfer (CT) states. The lower energy CT(S) state possesses D1 → A through-space CT nature with optically forbidden transition, while the higher lying CT(B) state is associated with optically allowed D2 → A CT through π-conjugation transition. Upon S_0 → CT(B) excitation, the charge transfer creates $D2^{\delta+}A^{\delta-}$ dipolar changes and $A^{\delta-}$-D1 repulsion, leading to structural relaxation of the CT(B) state that competes with fast CT(B) → CT(S) internal conversion. Therefore, despite the fact that they originate from the same Franck-Condon excited state, both energy stabilized CT(B) and CT(S) states are populated through two independent channels. The stabilized CT(B) and CT(S) states possess different optimized geometry and do not interconvert during their lifespans, rendering different population decay time constants. The slim HOMO/LUMO overlapped D1-A CT(S) state exhibits thermally activated delayed fluorescence (TADF), the character of which was further exploited as a host in OLED. The results gain new insights into the properties of the bending type D-D-A TADF triads. **CTPS** should not be a unique case. Bizarre photophysical behavior encountered in molecules comprising of multiple D and A groups may involve the interplay among various local CT states, which might have been overlooked.

INTRODUCTION

The triad types of molecular composites comprising various combination of electron donor (D) and acceptor (A) functional moieties, such as D-D-A, D-A-A, D-A-D, A-D-A, etc., have been attracting great attention in organic solar energy cells, organic light emitting diode (OLED) and a number of other applications.[1-3] These triads, being endowed with possible charge transfer (CT) and bipolar character in nature, are believed to either extend the light-harvesting spectrum or facilitate the electron/hole transporting properties to boost the device performance. Through ingenious design, some even exhibit thermally activated delay fluorescence (TADF) that gains much more efficiency than regular fluorescence OLEDs.[4-7] However, due to the molecular complexity, their photophysical properties are commonly sophisticated and may thus give rise to dual or even multiple emissions. Unfortunately, the origins of multiple emissions are often downplayed,[8-15] which, to certain extents, is tolerable if the consequence of application is significant. Indeed, in terms of OLEDs, the triad type of molecules has demonstrated great potential in practical applications.[3, 16-18]. However,

as for the long-term development, the lack of fundamental insight, especially the mechanism regarding excited-state relaxation dynamics that are responsible for the associated photophysical behavior, may deter the progress of rational molecular design and hence curb the advance in application.

Yet from another angle of view, via simply mixing D and A, the formation of exciplex with profound TADF property has demonstrated great potential of OLED application.[19-24] Due to the nature of intermolecular through-space CT, the slim orbital overlap between HOMO and LUMO in exciplexes renders small electron exchange energy and thus diminutive S_1-T_1 energy gap (ΔE_{ST}), for which TADF properties are commonly observed and used as either emitter or host materials for efficient energy transfer.[25-26] However, despite exciplex being a great candidate of host material for phosphorescent OLED, precisely controlled deposition of donor and acceptor materials for effective exciplex formation is required in order to minimize Langevin recombination process[27-28] and maximize Dexter-type energy transfer efficiency[29]. In this regard, we then manage to exploit the exciplex-like formation within a molecule composite,

which intrinsically takes advantage of intramolecular TADF property with precise donor/acceptor composition. As such, a facile intramolecular exciplex-TADF host material can be achieved. In theory, this approach may be virtually equivalent to a through-space type of intramolecular CT with intrinsic TADF, which, to the best of our knowledge, is new and its use of host material for phosphorescent OLED is unprecedented.

To attain this goal, in this study, 2-(4-(1-(4-(diphenylamino)phenyl)-9H-carbazol-9-yl)phenyl) dibenzothiophene sulfone (**CTPS**, **Scheme 1**) was designed and synthesized such that the donor triphenylamine (D1) and the acceptor dibenzothiophene sulfone (A) bridging through a rigid and coplanar donor carbazole (D2), arranging into a U-shape configuration. The rigidity of carbazole was introduced to prevent the perturbations from the conformational changes in the bridge unit. This configuration renders a face-to-face alignment between D1 and A and hence a potential for the photoinduced through-space charge transfer.

We have then performed comprehensive studies to illuminate the excited-state photodynamics of this D1-D2-A triad system. Unexpectedly, in solution, **CTPS** exhibits prominent dual emissions engendered by through-bond carbazole (D2)-dibenzothiophene sulfone (A) charge transfer and through-space triphenylamine (D1)-dibenzothiophene sulfone (A) charge transfer process. Such dual emissions within a single molecule are fascinating in their fundamental origin and potential applications.[30-45] The results show anomalous excitation-wavelength dependent ratiometric emissions, for which the mechanism incorporating anti-Kasha rule should be extendable to other multiple donor-acceptor composites. Detailed insights into the chemistry, photophysics and application in OLEDs are elaborated in the following sections.

RESULTS AND DISCUSSION

Synthesis.

For the design of D-D-A molecules, a rigid bridge donor is required to lock the distance between another donor and the acceptor. Carbazole was selected as the bridge skeleton because of its high rigidity and facile substitution in 1-position (see **Scheme 1**). Also, triphenylamine (**TPA**) acted as the second electron donor, while dibenzothiophene sulfone was selected as the acceptor moiety. Note that unlike some triads investigated in the past by Devens Gust and T. Moore with essentially no coupling between each donor and acceptor[46-47], the current triad, both based on the structural formula and dihedral angles, is a weakly coupled system.

Scheme 1 depicts the synthetic routes for **CTPS** as well as **CPS** and **CTS**. The key donor compound 1 was synthesized by the Suzuki coupling between 1-bromocarbazole and 4-(diphenylamino)phenylboronic acid. The acceptor fragment 2 was synthesized by a selective Suzuki coupling reaction of dibenzothiophene-2-boronic acid and 1-bromo-4-iodobenzene followed by the oxidation of dibenzothiophen with mCPBA. The final compound **CTPS** was then prepared by Buchwald-Hartwig coupling between 1 and 2 with a moderate yield of 45%. The reference compound **CPS** was synthesized according to the Suzuki coupling between 2-bromodibenzothiophene sulfone and 9-(4-(4,4,5,5-tetramethyl-1,3,2-dioxaborolan-2-yl)phenyl)-9H-carbazole. The other reference compound **CTS** was synthesized by reacting compound 1 with 2-bromodibenzothiophene sulfone catalyzed by Pd$_2$(dba)$_3$ in the presence of [1,1'-

biphenyl]-2-yldicyclohexylphosphine. All the newly synthesized materials were purified by column chromatography and vacuum sublimation before performing characterization and device fabrication. Detailed synthetic methods and analytical data are elaborated in the Supporting Information (SI).

Scheme 1. Synthetic routes of CTPS, CPS and CTS
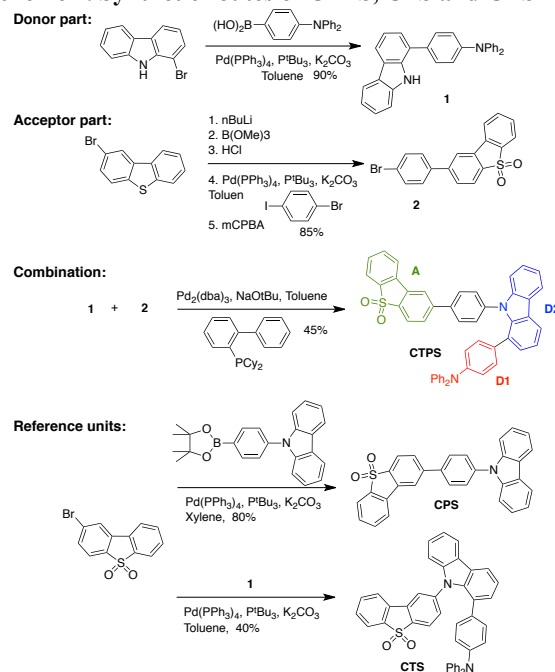
The molecular structures of **CTPS** and **CTS** were confirmed by ^{1}H NMR, mass and elementary analyses (see SI) as well as the single crystal X-ray diffraction method shown in **Figure 1**. The twist angles between carbazole (D2) and triphenylamine (D1)/D2 and dibenzothiophene sulfone (A) are 59.6 °/61.8° for **CTPS** and 54.5°/57.5° for **CTS**. Having similar twist angles, D1 and the acceptor unit nearly face to each other for both compounds. The distances between the N atom of triphenylamine (D1) and S atom of dibenzothiophene sulfone (A) were 6.73 Å and 5.64 Å for **CTPS** and **CTS**, respectively. The shorter distance between D1 and acceptor in **CTS** implies that the through-space electronic coupling between D1 and A moiety would be larger than that of **CTPS** (vide infra). **Figure 1 (b)** and **(d)** show the packing modes of **CTS** and **CTPS**. The distances between the neighboring donor and acceptor in **CTS** and **CTPS** are 8.89 Å and 7.39 Å, respectively. The large distance thus eliminates the intermolecular electronic coupling, rendering only electrostatic repulsive interactions between adjacent molecules for both compounds.
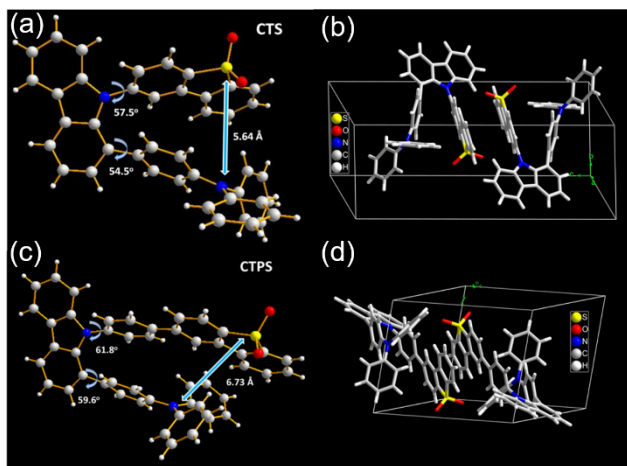
Figure 1. X-ray crystal structure of CTS ((a) and (b)) and CTPS ((c) and (d)).

Photophysical properties.

The steady-state UV-vis absorption, photoluminescence (PL) emission of **CTPS** in various solvents are shown in **Figure 2**. In cyclohexane, toluene and dichloromethane (DCM), dual emission bands are clearly observed. Pertinent spectroscopic data of **CTPS** in different solvents are listed in **Table 1**. For clarity, several remarks of the results are pointed out below, followed by corresponding discussion.

i. The dual emission bands, specified as F1 and F2 for short and long wavelength bands, respectively, are both subject to significant solvatochromism. For example, the peak wavelengths 370 nm and ~460 nm for F1 and F2 in cyclohexane are red shifted to ~450 nm and 570 nm, respectively, in DCM, manifesting their charger transfer character in nature.

ii. In all solvents applied, the intensity ratio for the F1 versus F2 band greatly changes from aerated to degassed solution. In comparison to spectra in the aerated solution (**Figure 2(a)**), the emission intensity of the F2 band is enhanced by several folds upon degassing while the F1 band remained unchanged (**Figure 2(b)**). The F2 band, being quenched by O$_2$, implies its possible TADF property. This is also evidenced by the decay kinetics of F2 band (monitored at 500 nm) in e.g., the degassed toluene, which revealed an exceedingly long decay component of ~100 μs, and is drastically quenched to as short as 15 ns upon aeration (see **Table 1** and **Figure S5**).

iii. In either aerated or degassed toluene solution, the normalized excitation spectra monitoring for **CTPS** at different wavelengths are different (**Figure 3**). This difference cannot be attributed to the solvent (toluene) interference[48] because of negligible absorption at > 300 nm for toluene. Moreover, the monitored emission wavelength dependent excitation spectra were also observed in other solvents, for which the corresponding solvents such as cyclohexane and dichloromethane virtually have no absorption at > 300 nm (see **Figure S6** in SI). Likewise, as shown in **Figure 3** (and **Figures S7** and **Table S1** for degassed solution), the intensity ratio for F1 versus F2 emission bands is excitation wavelength dependent, having maximum ratio upon 340 nm excitation and decreasing on either decrease or increase of excitation wavelength. This observation is anomalous, which, in a sense, demonstrates an exceptional case defying Kasha's rule stating that independent of the excitation wavelength, emission of molecules in the condensed phase has to be

from the lowest lying singlet (fluorescence) or triplet (phosphorescence) manifolds.[49]
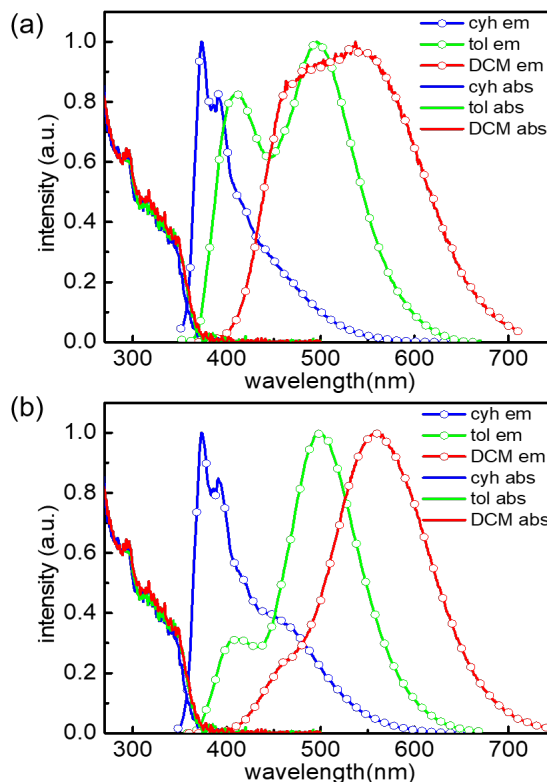
Figure 2. Absorption and emission (λ_{ex} = 340 nm) spectra of **CTPS** in (a) aerated and (b) degassed cyclohexane (blue line), toluene (green line), and DCM (red line).
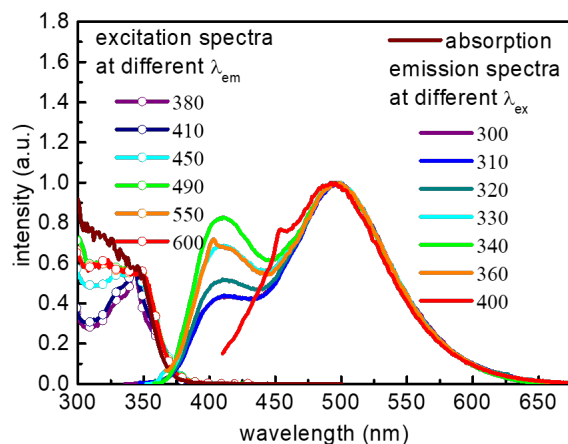
Figure 3. Excitation (monitored at indicated emission wavelengths), absorption, and emission spectra (excited at indicated wavelengths) of **CTPS** in aerated toluene.

To gain more insight into the photophysical properties of **CTPS**, **Figure 4** shows the comparative absorption and emission spectra for **CTPS** and the reference molecules **CPS**, **CTS** (see **Scheme 1**) and triphenylamine (**TPA**) in toluene. The corresponding time-resolved spectroscopic data are listed in **Table 1**, **Table S2** and **Table S3**. Chemically, the combination of **CPS** and **TPA** constructs **CTPS**. As shown in **Figure 4**, although the

Table 1. Steady-state and time-resolved spectroscopic data of CTPS in different solvents. All the data are obtained when λ_{ex}= 340 nm.

solvent	Emission peak [nm] [a]	Q.Y. [%][c]	$\lambda_{monitor}$[nm]	Fitted time constants [ns] [a] (prefactor)	Fitted time constants [ns] [b] (pre-exponential factor)
cyclohexane	370, 460	43.1[a],47.5[b]	370	1.75 (-)	1.81 (-)
			420	2 (0.91), 6 (0.09)	1.81 (0.999), 33.72 (0.001), > 10^5 (< 10^{-3})
			450	2 (0.55), 6 (0.45)	1.81 (0.976), 33.72 (0.024), > 10^5 (< 10^{-3})
toluene	410, 500	7.43[a], 10.8[b]	400	2.31 (-)	2.31 (-)
			450	2.31 (0.88), 15 (0.12)	2.31 (0.93), 56.89 (0.07), > 10^5 (< 10^{-3})
			500	2.31 (0.19), 15 (0.81)	2.31 (0.77), 56.89 (0.23), > 10^5 (< 10^{-3})
DCM	450, 570	3.13[a], 8.85[b]	480	5.5 (0.98), 37 (0.02)	2 (0.985), 160 (0.015), > 10^5 (< 10^{-3})
			575	5.5 (0.32), 37 (0.68)	160 (~1), > 10^5 (< 10^{-3})

[a] measured in aerated solution. [b] measured in degassed solution. [c] emission quantum yield

absorption spectrum of **CTPS** is similar to the sum of the absorption of **CPS** and **TPA**, a slight difference at the spectral onset of 390-420 nm (see insert of **Figure 4**) is noticeable, indicating a rather small but non-negligible electronic coupling between **CPS** and **TPA** moieties in forming **CTPS**. The F1 emission band of **CTPS** matches well with the emission of **CPS** in terms of spectral feature (400 nm), emission lifetime (2.31 ns in toluene) (see **Table 1**) and solvatochromism (cf. **Figure 2** and **Figure S8**). This leads us to conclude the same CT transition nature for the **CTPS** F_1 band and **CPS** emission, which most plausibly originates from CT from carbazole (D2) to dibenzothiophene sulfone (A, **Scheme 1**). Such a D2 → A CT is presumably through a π-conjugation and hence the electron coupling constant is large. In other words, **CTPS** possesses an allowed optical electron transfer state, defined as the CT(B) state that exhibits solvent polarity dependent F1 emission band.
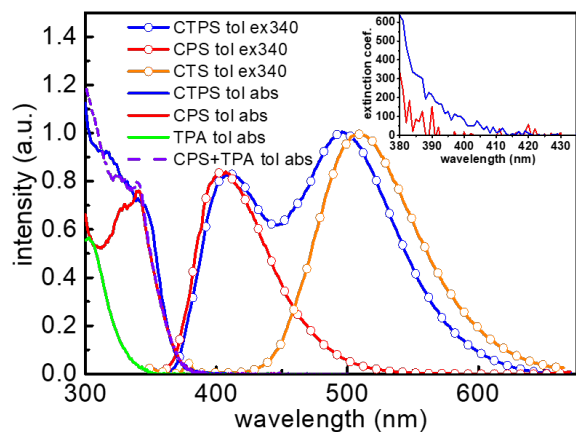
Figure 4. Absorption and emission spectra (λ_{ex}=340 nm) of **CTPS**, **CPS**, **CTS** (only emission) and **TPA** (only absorption) in aerated toluene. The purple dash line is the summarized spectrum of the absorption for **CPS** and **TPA**. The insert is the absorption spectra of **CPS** and **CTPS** zoomed in the region of 380-440 nm.

On the other hand, **TPA** virtually has no emission in any solvents; therefore, the contribution of the **CTPS** F2 band solely from the **TPA** moiety is eliminated. This also discards the proposal that **CPS** and **TPA** are mutually orthogonal, giving F1 and F2, respectively. We then made a comparison between the F2 band of **CTPS** and the emission of **CTS** (**Figure S9, Figure S10** and **Table S3**, see **Scheme 1** for structure). In toluene, single emission band maximized at ~500 nm was observed for **CTS**, which is nearly identical with the F_2 band (500 nm). Moreover, **CTS** also undergo similar trend of solvatochromism as the F2 band of **CTPS**, being red shifted from 450 nm in cyclohexane to 550 nm in CH₂Cl₂. These, together with the similar population decay time between **CTPS** (F_2 band, 15 ns in toluene) and **CTS** emission (21 ns in toluene), indicate a similar type of charge transfer property. Later we will verify that **CTS** undergoes exclusively **TPA**(D1) →dibenzothiophene sulfone (A) CT transition (vide infra). Accepting this consequence, the F_2 band thus originates from a D1 → A CT via the electronic coupling between **TPA** and dibenzothiophene sulfone moieties (**Scheme 1**) in a "through space" manner. This through-space CT state, defined as the CT(S) state, infers its slim HOMO/LUMO overlap. As a result, the small electron exchange energy results in a small energy gap, ΔE_{S-T}, between S1 and T1 states, rationalizing the TADF property of the F_2 band. In comparison, the lack of TADF property for the F_1 band (from the CT(B) state) can be understood by its through π-conjugated CT character with a significant HOMO/LUMO overlap. The net result is to increase the electron exchange energy and hence a large ΔE_{S-T} gap to prohibit TADF. Further insight into the orbital configuration for both CT(B) and CT(S) states will be discussed in the section of theoretical approach.

In a brief summary, F_1 and F_2 bands in **CTPS** originate from two different CT states specified as CT(B) and CT(S) states, possessing D2 → A and D1 → A type CT character, in which B and S denote through-π-conjugated bridge and through-space CT in nature, respectively. CT(B) is in the higher energy state and S_0 → CT(B) is an optically allowed process, while CT(S) is in the lowest lying excited state, for which S_0 → CT(S) is

only partially allowed with rather small oscillator strength. The latter is also supported by the small absorption tail in **CTPS**, with ~100 $M^{-1}cm^{-1}$ absorption extinction coefficient appearing at 400 nm that is not observed in **CPS** (see inset of **Figure 4**).

The excitation wavelength dependent dual emission bands, together with two distinctly different population lifetime for F1 and F2 bands, is anomalous and of fundamental interest. It indicates that **CTPS**, upon Franck Condon excitation, undergoes two separated relaxation pathways that are irrelevant to one another. We have to emphasize that the two distinct and individual CT emissions reported here are apparently not the same as the dual emissions of the 'fruit-fly' molecule dimethylaminobenzonitrile originating from LE and TICT states. As reported previously,[50] only the TICT emission exhibits solvatochromism and the solvent polarity controls the relative populations of these two states. Further, in the study by Druzhinin, et al.,[51] the LE and CT states of dimethylaminobenzonitrile showed precursor-successor type relationship with same population decay lifetime, demonstrating that the interconversion between LE and CT states takes place. In current study, differently, the excitation wavelength dependent emission, different population decay lifetime, and the lack of precursor-successor type relationship of CT(S) and CT(B) state all indicate that the interconversion between CT(S) and CT(B) states of CTPS cannot take place, which is new and previously unrecognized. To gain more understanding into this unusual excited-state dynamics, we then applied the femtosecond fluorescence up-conversion measurement in attempts to resolve the associated kinetics and temporal evolution of photoluminescence spectra (**Figure 5**). Pertinent fitting data are summarized at **Table 2**. **Figure 5** shows both temporal spectral evolution and the trace of emission dynamics under 360 nm excitation. Due to the limit of light source, 360 nm laser pulse is the shortest wavelength accessible to the lower lying excited states of **CTPS**. Therefore, the shortest emission wavelength that is able to be monitored free form scattering-light interference is 420 nm. Upon monitoring at 420 nm, the kinetic trace is composed of a rise component with a time constant fitted to be 6.2 ps, followed by a nearly constant value within the acquisition time window of 100 ps; the latter indicates a long population decay time, which is further resolved by time-correlated single photon counting (TCSPC, see inset of **Figure 5 (b)**) system to record a lifetime of 2.3 ns. The relaxation time constant for toluene is known to be 1.05 ps at room temperature[52]. In addition, the energy gap between the excitation wavelength (360 nm) and monitored emission (420 nm) is rather small. Therefore, it is very unlikely that the 6.2 ps rise time constant is ascribed to the solvent or vibrational relaxation. Instead, more plausibly, the 6.2 ps time constant is associated with the structural relaxation dynamics of the optically allowed CT(B) state. Further support of this viewpoint is given by the computational approach (vide infra). On the other hand, the emission relaxation dynamics of the CT(S) state, monitored at 510 nm (the F2 band), consists of a 12.5 ps rise component and a constant value within 100 ps acquisition time window. The latter is further resolved by TCSPC to be as long as 15 ns (inset of **Figure 5 (c)**). The 12.5 ps rise component of the F2 band is nearly twice as long as that (6.5 ps) of the F1 emission band (cf. **Figure 5 (b)** and **5 (c)**) and thus cannot be ascribed to the solvent/vibrational relaxation for which the solvatochromism should take place within few ps. Due to the interference of the proximal F1 band, the solvatochromic evolution of the F2 band within few ps

could not be resolved. However, even after few ps, as shown in **Figure 5 (a)**, the time-resolved F2 spectra still exhibit a red-shifted emission from 485 nm to ~500 nm within a time window from 2.5 ps to 30 ps, which cannot be ascribed to the temporal evolution from solvatochromism. Thus, it is reasonable to assign the 12.5 ps as the time constant to stabilize the CT(S) state via a slower relaxation process. As a result, the ultrafast spectroscopies demonstrate the existence of a relatively slow structural relaxation for both CT(B) and CT(S) states. Further theoretical approach elaborated below affirms the relevant motion.
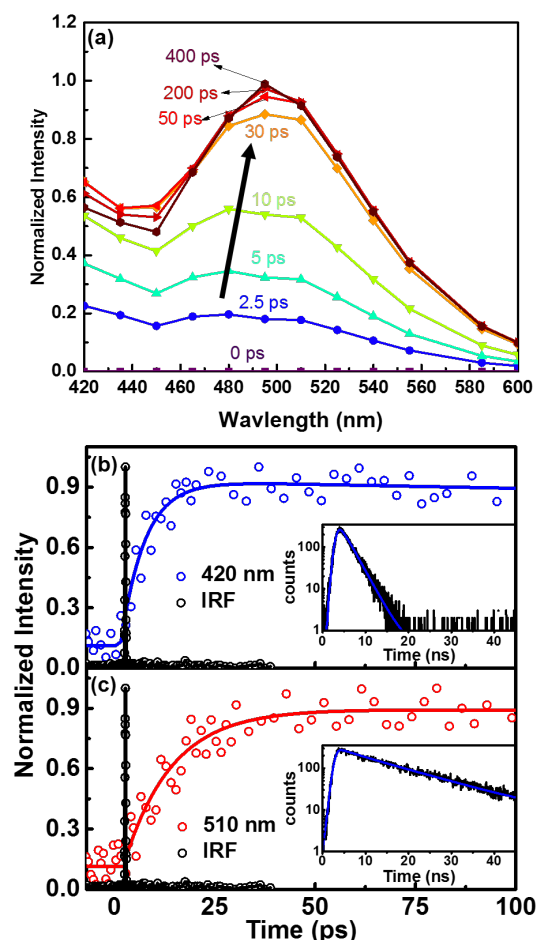
Figure 5. (a) Time-resolved photoluminescence spectra (b) Fluorescence up-conversion measurement of **CTPS** in toluene monitored at indicated emission wavelengths. λ_{ex} =360 nm. Inset: The nanosecond population decay trace at indicated wavelength by TCSPC measurement. IRF: the instrument response function

Table 2. Fitting data of the fluorescence up-conversion measurement of CTPS in toluene.

λ_{ex} [nm]	$\lambda_{monitor}$ [nm]	Fitted time constants [ps] (pre-exponential factor)
360	420	6.2 (-0.544), 2,300 (0.456)
	510	12.5 (-0.478), 15,000 (0.522)

Theoretical approaches

To rationalize the above results and to testify the proposed mechanism, we then carrried out comprehensive theoretical calculation. In this approach, the geometry optimization on the ground-state, S_1, and S_2 states of **CTPS** as well as the transition properties were performed by cam-B3LYP functional associated with the 6-31+G(d,p) basis sets in toluene environment. **Figure 6 (a)** depicts the optimized molecular structures in the ground state for **CTPS** where the HOMO-1, HOMO, and LUMO mainly localize at carbazole (D2), triphenylamine (D1) and dibenzothiophene sulfone (A) moieties, respectively. In addition, **Figure S11** and **Table S4** summarize the orbitals involved in the excited states upon vertical transition. The calculated lowest lying excited state (S_1) is dominated by HOMO (D1) → LUMO(A), which, according to the configuration (**Figure 6**), is ascribed to be a "through-space electron transfer" and is manifested by its small oscillator strength of f=0.0425. State congestion was obtained among S_2-S_4 states due to their proximal energy levels, in which HOMO-1 (D2) → LUMO (A) transition, a through π-conjugation electron transfer, is dominant, as supported by a large oscillator strength f=0.2393. Thus, via Franck Condon excitation, the unrelaxed S_1 and S_2 states possess a through space and a through π-conjugation CT character, respectively.
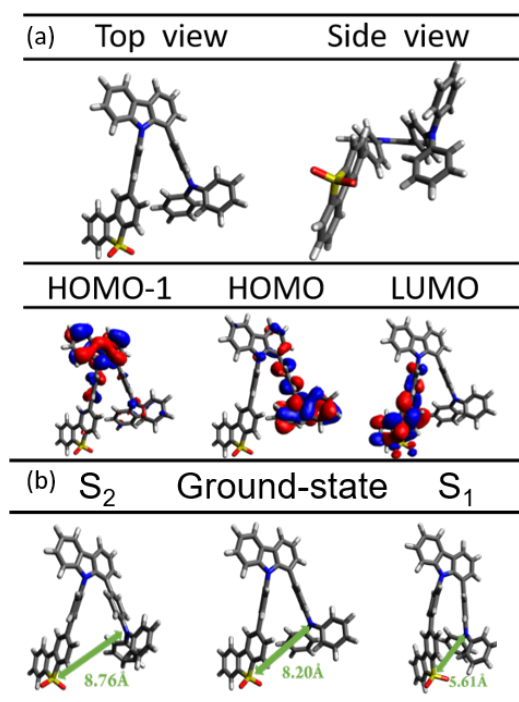
Figure 6. (**a**) Optimized molecular structure in the ground state and the associated frontier orbitals for **CTPS**. (**b**) The distance d_s, which is defined by the distance between the nitrogen atom on D1 to the sulfur atom on the A moiety (see **Figure 1** for definition), for the optimized structure of **CTPS** in S_0, S_1 and S_2 states.

Full geometry optimization of S_1 and S_2 states was then carried out to analyze the associated emission properties. As a result, comparing **Figure 6 (a)** and **Figure S12**, there are no dif-

ferences in the associated frontier orbital configurations for optimized S_1 and S_2 states, which are unambiguously assigned to S_1(CT(S)) and S_2 (CT(B)) with D1 → A and D2 → A transition characteristic. However, the optimized geometry among S_0, S_1, and S_2 states are rather distinct, particularly in terms of through-space distance between D1 and A, d_S, which is defined by the distance between the nitrogen atom on D1 to the sulfur atom on the A moiety (**Figure 6 (b)**). Compared with d_S of 8.20 Å for the S_0 state, d_S of 5.61 Å of the stabilized S_1 (CT(S)) state is significantly shorter. Conversely, d_S of the optimized structure of CT(B) is elongated to as larger as 8.76 Å. The large difference in d_S among S_0, CT(S) and CT(B) states are intriguing, which, in a qualitative manner, can be rationalized by the divergence of the static interaction amid the charge transfer. The S_2 (CT(B)) state possesses a $D2^{\delta+}A^{\delta-}$ character that aggravates $A^{\delta-}$-D1 (electron rich) repulsion (see **Figure 6 (b)**). In sharp contrast, the through-space CT S_1 state induces the attraction between $D1^{\delta+}$ and $A^{\delta-}$ (**Figure 6 (b)**) hence the gradual reduction of the d_S via structure relaxation. Moreover, the calculated oscillator strengths f of 0.77 and 0.005 for S_2 (CT(B)) and S_1(CT(S)) clearly indicate very small electronic coupling matrix between S_2(CT(B)) and S_1(CT(S)). This viewpoint can be clearly visualized by the separation of the frontier orbitals on two different donors (see **Figure 6 (a)**).

In light of above experimental and theoretical approaches, we herein propose a rational mechanism, depicted in **Figure 7**, to account for the excited-state properties of **CTPS** in solution. To simplify the complex state congestion, we first assume the 360 nm excitation (absorption peak of **CTPS**) to be the pure, optically allowed $S_0 \rightarrow S_2$(CT(B)) excitation for **CTPS** (see blue line in **Figure 7**). The optical $D2^{\delta+}A^{\delta-}$ charge transfer in the S_2 state instantly induces the solvent stabilization that theoretically takes place in less than few ps. As elaborated above, the S_2(CT(B)) state then undergoes two competitive relaxation pathways. On the one hand, the $A^{\delta-}$-D1 repulsion leads to structural relaxation mainly along the spatial coordinate d_S. On the other hand, the S_2(CT(B)) → S_1(CT(S)) internal conversion takes place, involving $D2^{\delta+}A^{\delta-} \rightarrow D1^{\delta+}A^{\delta-}$ charge transfer, solvent stabilization, followed by structural relaxation to reduce the spatial distance d_s owing to the attraction between $D1^{\delta+}$ and $A^{\delta-}$ moieties in the S_1(CT(S)) state. Despite their origin from the solvent stabilized S_2(CT(B)) state, these two opposite structural relaxation pathways, i.e. the elongation and reduction of d_s, have their subsequent different relaxation dynamics, resulting in two independent pathways.

Once reaching the structurally relaxed S_2(CT(B)) and S_1(CT(S)) states, herein denoted as S(CT(B))$_{relax}$ and S(CT(S))$_{relax}$, respectively, the much different d_s of these two stabilized geometries, together with their very weak electronic coupling, makes the interconversion between S(CT(B))$_{relax}$ and S(CT(S))$_{relax}$ states kinetically prohibitive within their emission lifespan. The net result gives two emission bands having CT and hence prominent solvatochromism properties with distinct photophysical properties. For the S(CT(S))$_{relax}$ state the slim HOMO/LUMO overlap renders small electron exchange energy. Thus, a close energy gap ΔE_{S-T} between S_1 and T_1 is expected, which is estimated as ~2.4 kcal/mol (0.10 eV) by the energy

difference in peak frequency between fluorescence and phosphorescence (**Figure S13**), rationalizing the TADF property of the S(CT(S))$_{relax}$ emission.
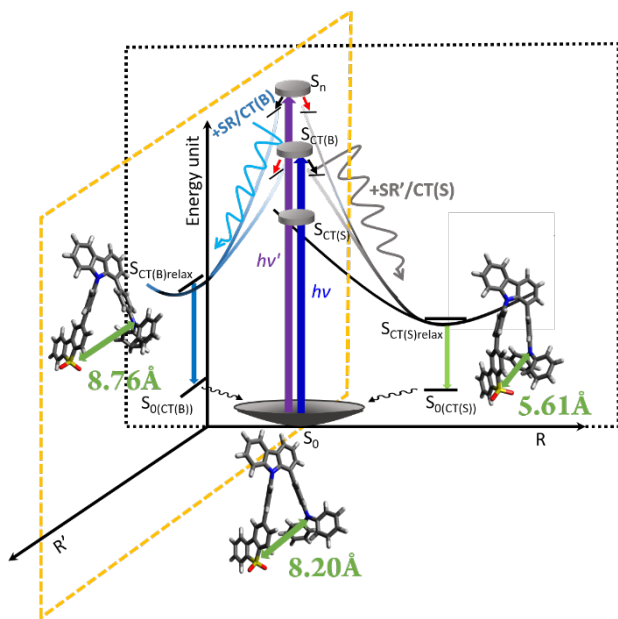
Figure 7. A schematic diagram illustrating the photodynamics of **CTPS** in toluene upon photoexcitation. (R and R': structural coordinate; SR denote structural relaxation).

The above scenario is based on the simplification that the 360 nm excitation is ascribed to the pure $S_0 \to S_2$(CT(B)) transition. In reality, state congestion was recognized among S_2-S_4 states due to their proximal energy levels (vide supra). Also, there should be a mixing between the initially prepared S_2(CT(B)) and highly vibronic S_1(CT(S)) state. These lead to the complication in the population branching ratio for S_2(CT(B)) $\to$ S(CT(B))$_{relax}$ versus S_2(CT(B)) $\to$ S(CT(S))$_{relax}$ processes. In other words, the population ratio for S(CT(B))$_{relax}$ versus S(CT(S))$_{relax}$ is expected to be excitation energy dependent, as evidenced by the steady-state result depicted in **Figure 3**. Unfortunately, the support from early relaxation dynamics is pending due to the limit of current femtosecond light source to produce 300-350 nm excitation.

In solid film and application for OLED.
    Prior to exploring the applications of **CTPS** and **CTS**, the characteristics in solid films were examined. As shown in **Figure 8**, **CTPS** exhibits a single emission band maximized at 513 nm. In addition, TADF is clearly observed, consisting of a prompt and a delayed emission component of 96.1 ns and 0.365 μs, respectively (inset of **Figure 8** and **Table S5**). According to the photophysical properties in solution, such long population lifetime with TADF character, along with the emission peak near 510 nm, suggests that this single emission in solid film originates from the S(CT(S))$_{relax}$ state. In addition, the results indicate that certain structure relaxation takes place in the soft-packed film prepared by evaporation, in a kinetic manner, so that the S(CT(S))$_{relax}$ state is populated. Furthermore, the solid film creates a more rigid environment for **CTPS** molecules that inhibits the formation of S(CT(B))$_{relax}$ state which requires the

elongation of distance between the nitrogen atom on D1 to the sulfur atom on the A moiety within **CTPS**, rendering only the emission of S(CT(S))$_{relax}$ state. On the other hand, shown in **Figures 8** and **Table S5**, **CTS** also reveals TADF properties in vapor deposited film with similar emission peak wavelength at 518 nm. This can be rationalized by the shorter d_s of ~5.64 Å for **CTS** in crystal (cf. 6.71 Å for **CTPS** in crystal, **Figure 1**), so that D1 → A charge transfer can take place efficiently in film as well as solution because of small inner reorganization energy.
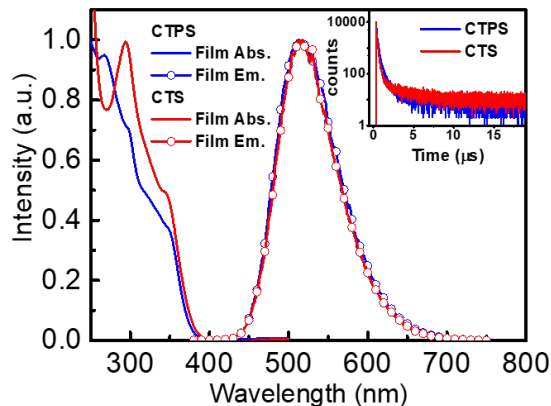
Figure 8. The absorption in solid film (solid line) and emission in vapor deposited film (circle solid line) for **CTPS** and **CTS**. Inset: Lifetime measurement of **CTPS** and **CTS** in solid film at room temperature.

Figure 9 (a)-(b) demonstrates the temperature dependent lifetime measurement of **CTS** and **CTPS** film. When the temperature rises, unlike some well-known TADF compounds (e.g. DMAC-TRZ,[53] **Figure S16**) which demonstrate more delayed TADF component (the long decay component), both **CTPS** and **CTS** exhibit less TADF component. To rationalize this phenomenon, we conducted the simulation of TADF kinetics (see **Figure 9 (c)-(d)** and **Figure S17**) to gain further insight into the TADF dynamics of **CTS** and **CTPS** in solid film. As a result, when the temperature rises, the rate of reverse intersystem crossing (k_{risc}) increases, which directly increases the rate of TADF and hence augments the TADF component as shown in **Figure S17 (b)**. However, concurrently, the simulation also indicates that the non-radiative decay rate of the excited state would also be boosted, which increases the population decay rate of S_1 (k_f) that is about 2 order of magnitude faster than k_{risc}. The increase of k_f leads to faster prompt fluorescence rate and thus more component of prompt fluorescence concomitant with less TADF component as depicted in **Figure S17 (c)**. Therefore, it is the interplay between the temperature dependent k_{risc} and k_f that determines the increase or decrease of the TADF component as the temperature varies. In this regard, as the exemplar, the kinetic rates of **CTS** at -100 °C and 50 °C are obtained and depicted in **Figure 9 (c)-(d)** from the fitted data shown in **Table S6**. The fitted change of k_f from 5×10^6 s^{-1} (-100 °C) to 10^7 s^{-1} (50 °C) dominates in the temperature effect, rendering less TADF component as the temperature rises (see **Figure 9 (a), (d)**). As a result, the excited-state dynamics of **CTS** is accordant to the TADF properties in solid film. With similar results (cf. **CTS**) of temperature dependent lifetime measurement, **CTPS**,
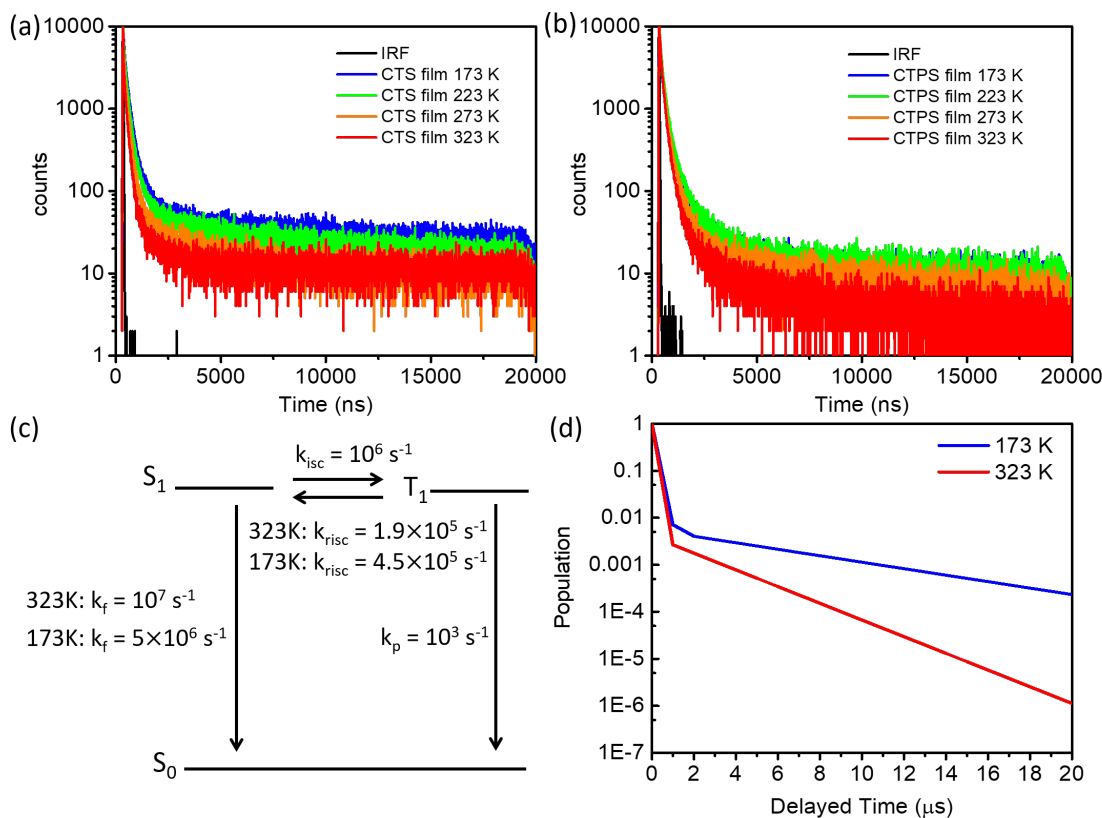
Figure 9. Lifetime measurement of **(a) CTS (b) CTPS** film at indicated temperatures. **(c)** TADF kinetics of **CTS** film. k_f: the derived population decay rate of S_1. k_p: the population decay rate of T_1. k_{isc}: the rate of intersystem crossing. k_{risc}: the rate of reverse intersystem crossing. **(d)** The simulated S_1 population change of **CTS** film at 173 K and 323 K.

exemplified by the analysis of **CTS**, is also corroborated to possess TADF property. For the bending type TADF molecules **CTPS** and **CTS** studied here, k_f may be subject to the quenching of the small frequency bending motion that is temperature dependent and thus influences the observed relaxation dynamics. This uncommon temperature dependent excited-state dynamics due to the bending D-D-A alignment should not be overlooked, which may gain more new insights into TADF fundamental.

In the pristine solid film, the emission yield, Q.Y., of **CTPS** and **CTS** was measured to be 23.64% and 33.94%, respectively. The relatively lower Q.Y. for **CTPS** (cf. **CTS**), could be rationalized by the more degrees of freedom of small amplitude torsional motions for **CTPS**. To further understand the charge-carrier transport properties, we used the time-of-flight (TOF) technique to evaluate the carrier mobility. **Figure S18 (a)-(c)** displays typical room-temperature TOF transient photocurrents under an applied electric field. The transit time, τ_T, can be evaluated from the intersection point of two asymptotes in the double-logarithmic representation of the TOF transient. **Figure S18 (d)** shows the field dependence of carrier mobilities follows the nearly universal Poole-Frenkel relationship within the range from 3.0×10^{-7} to 1.4×10^{-5} cm^2 V^{-1} s^{-1} for fields varying from 1.7×10^5 to 2.0×10^6 V cm^{-1}. Apparently, the distance between carbazole and dibenzothiophene sulfone has a crucial influence

on the charge transport behavior. **CTS** has bipolar charge-transport properties with more balance electron/hole mobilities. In contrast, the transient photocurrent signals of **CTPS** for electrons were too weak for us to evaluate electron mobility.

Table 3 and **Figure S18** lists the physical and photophysical parameters of **CTPS** and **CTS** in the solid film required for OLEDs. OLEDs based on **CTPS** and **CTS** as the pure emitters as well as 10 wt% dopants into mCPCN host[54] in emitting layer were performed. The results listed in **Table S7** and **Figure S19** are not impressive, with EQE of 1.87% (**CTS**), 2.7% (10wt% **CTS**: mCPCN), 0.87% (**CTPS**) and 2.55% (10wt% **CTPS**: mCPCN) for a number of configurations being tested. This is perhaps due to rather low PLQY, as well as poor mobility in both electron and hole for both **CTPS** and **CTS (see Table 3** and **Figure S18)**. Nevertheless, **CTPS** and **CTS** proved to be promising candidates for serving as the electrophosphorescence hosts because of their TADF nature, that can facilitate the harvest of electro-generated triplet excitons followed by triplet-triplet energy transfer to reach to phosphorescent dopants for efficiently relaxing the excited states and thus giving high efficiency devices. In this approach, we fabricated PhOLED devices with four phosphors respectively, including green bis(2-phenylpyridinato)-iridium(III) acetylacetonate (PPy)$_2$Ir(acac)[55],

Table 3. **The Physical properties of CTS and CTPS in solid film.**

	HOMO (eV)[a]	LUMO (eV)[a]	ΔE_g (eV)	λ_{abs} (nm) Solu.[b] /Film	λ_{em} (nm) Solu.[b]/Film	PLQY (%)	μ(cm²/Vs)[c]
CTS	-5.47	-2.21	3.26	294, 345/294, 345	514/514	33.94	(h) 2.3x10⁻⁶ (e) 5x10⁻⁷
CTPS	-5.54	-1.97	3.57	295, 347/297, 349	406, 500/ 521	23.64	(h) 3x10⁻⁷

[a] HOMO energy level determined by using photoelectron yield spectroscopy (AC-2). LUMO = HOMO + ΔE_g, where ΔE_g is calculated from the absorption onset of film state. [b] Measured in toluene. [c] Mobility under an electric field of 1.3 x 10⁶ V cm⁻¹.

yellow bis(2-phenylbenzothiazolato) (acetylacetonate)iridium-(IIh'I) (Bt)₂Ir(acac),[56] orange tris(2-phenylquinoline)-iridium(III) Ir(2-phq)₃,[57] and red [2-(3-methylquinolin-2-yl)phenyl](acetylacetonate)iridium(III) (Mpq)₂Ir(acac)[58] as dopants in the device structure: ITO/4% ReO₃: Tris-PCz (60 nm)/Tris-PCz (15 nm)/EML (25 nm)/BPhen (50 nm)/Liq (0.5 nm)/Al (100 nm). The device structure and the molecular structures of materials fabricating the device are shown in **Figure 10**. To lower the hole injection barrier from ITO to 9,9',9"-triphenyl-9H,9'H,9"H-3,3':6',3"-tercarbazole (Tris-PCz),[57] we used rhenium oxides (ReO₃) as a dopant material in Tris-PCz to produce ohmic contact.[59-60] Tris-PCz, 4,7-diphenyl-1,10-phenanthroline (BPhen), 8-hydroxyquinolinolatolithium (Liq), and Al were used as the hole-transporting layer (HTL), electron-transporting layer (ETL), electron injection layer (EIL), and cathode, respectively.
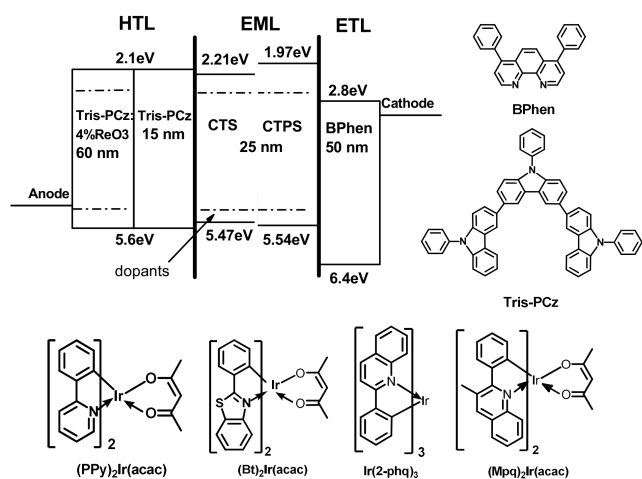
Figure 10. The device structure with energy level diagram and the molecular structures of functional materials used in devices.

As a result, **Figures 11** show the current density-voltage-luminance (*J-V-L*) characteristics, external quantum (EQE) and power efficiencies (PE) as a function of luminance as well as EL spectra of devices for CTS and CTPS as a host, respectively, with detail data shown in **Table 4**. The notation 1 and 2 indicates the devices fabricated with host materials of **CTS** and **CTPS**, respectively. All devices exhibited a low turn-on voltage (V_{on}) of 2.2 V. The **CTS** doped with (PPy)₂Ir(acac) device G1 revealed the best device performance, with the maximum external quantum (EQE), current (CE), and power (PE) efficiencies were 20.4%, 74.6 cd A⁻¹, and 90.6 lm W⁻¹, respectively. In addition, the roll-off of efficiency is extremely low compared to other studies of (PPy)₂Ir(acac) devices[61] with EQE of 19.1% at 1000 cd m⁻² (3.4 V) and 17.3% at 10000 cd m⁻² (4.3 V). The same trend can also be observed for **CTS** based device with different long-wavelength-emitting dopants. The yellow (Bt)₂Ir(acac) device Y1 can be achieved relatively high EL efficiencies (19.8%, 49.8 cd A⁻¹, and 59.8 lm W⁻¹). The Ir(2-phq)₃ O1 and (Mpq)₂Ir(acac) R1 devices exhibited relatively lower EQEs (16.3% and 15.3%). The devices displayed pure emission and there are no residual emissions from the host and/or adjacent layers in **Figure 11 (e)-(f)**, indicating that the electroluminescence is completed energy transfer from host to dopant.

However, devices with **CTPS** as host exhibit lower EL efficiencies and lower current density than the **CTS** hosted device. This can be attributed to only hole-transport of **CTPS** (**Figure S18**) and higher barrier between **CTPS** and BPhen (**Figure 10)** that leads unbalances of holes and electrons in EML. In addition, the luminescence property in solid film leads us to propose that the relatively lower Q.Y. for **CTPS** (23.64%, cf. 33.94% for **CTS** in solid film) limits the external quantum efficiency of the whole device, despite that the excitons in triplet state can be utilized. On the contrary, the **CTS**-based devices, with predominant TADF emission and higher Q.Y., render better OLEDs performance. Moreover, the solid film environment excludes the formation of S(CT(B))ᵣₑₗₐₓ state that lacks TADF property, engendering only S(CT(S))ᵣₑₗₐₓ state and thus exhibiting great OLED performance for devices with either **CTS** or **CTPS** acting as the host material.

Table 4. EL performances of devices with CTS and CTPS acting as host material.

	V_{on}[b] [V]	L/J at 8V [cd m⁻²/ mA cm⁻²]	EQE/CE/PE$_{max}$ [%/ cd A⁻¹/ lm W⁻¹]	EQE/V at 10³ cd m⁻²[c] [%/ V]	CIE [x,y]
G1[a]	2.2	24300/ 890	20.4/ 74.6/ 90.6	19.1, 3.4	0.31,0.63

	Turn-on[b]	Luminance	EQE	Power Eff.	CIE
Y1	2.2	164610/ 1325	19.8/ 49.8/ 59.8	18.7, 3.6	0.53,0.47
O1	2.2	111500/ 1140	16.3/ 30.6/ 39.2	15.0, 3.8	0.59,0.41
R1	2.2	47080/ 1224	15.3/ 13.5/ 18.2	13.6, 4.0	0.66,0.34
G2	2.2	22510/ 84	9.5/ 34.4/ 30.2	9.3, 5.0	0.32,0.63
Y2	2.2	68920/ 472	11.4/ 29.4/ 28.7	11.3, 4.0	0.53,0.47
O2	2.2	38620/ 406	9.4/ 17.0/ 18.3	9.1, 4.4	0.59,0.41
R2	2.2	19540/ 1762	10.9/ 10.0/ 11.0	10.1, 4.8	0.66,0.34

[a] The notation 1 and 2 indicate the devices fabricated with host materials of **CTS** and **CTPS**, respectively. [b] Turn-on voltage at which emission became detectable. [c] The values of driving voltage and EQE of device at 1000 cd m^{-2} are depicted in parentheses.
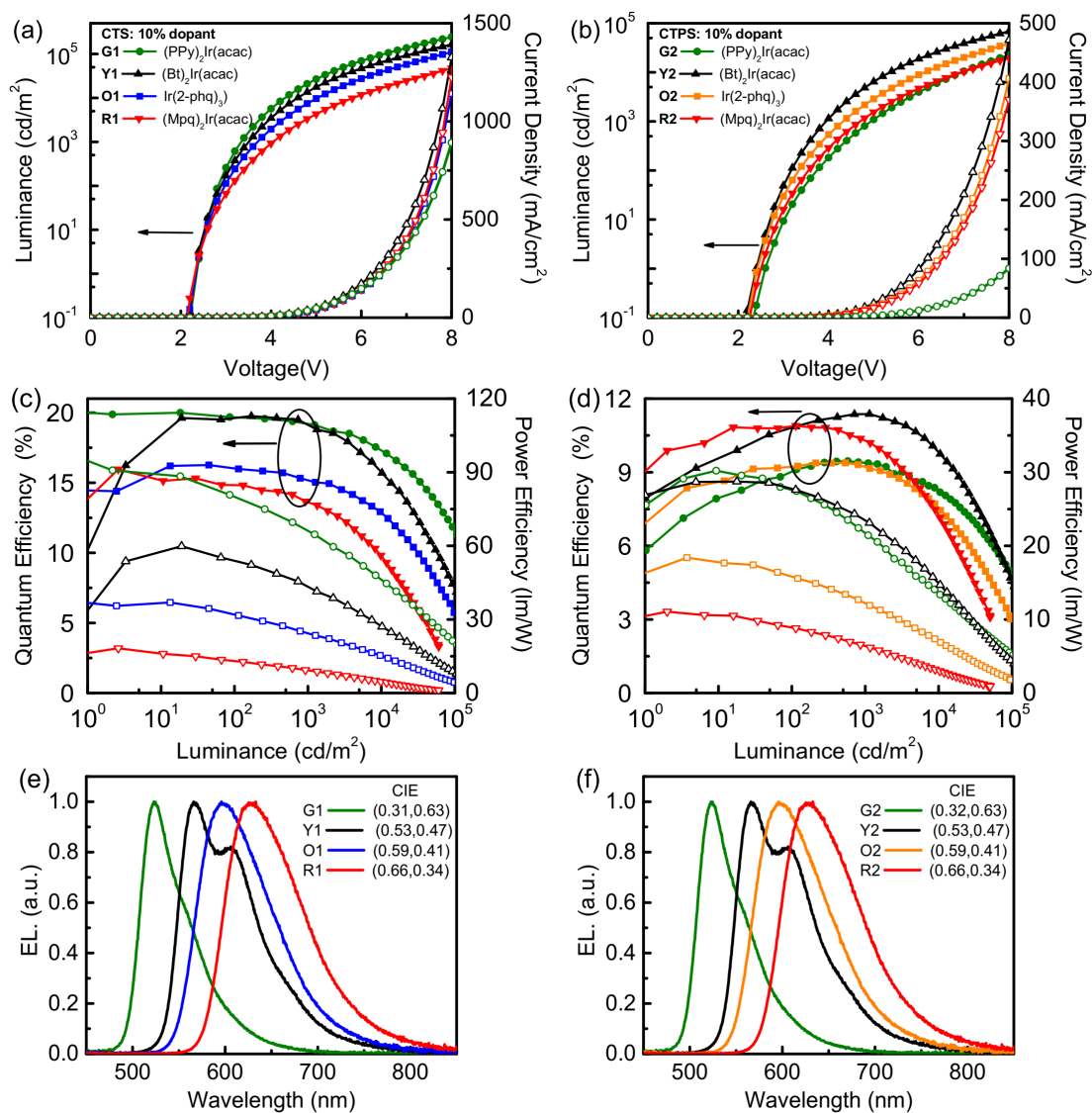
Figure 11. (a)(b) Current density-voltage-luminance (*J-V-L*) characteristics. (c)(d) External quantum (η_{ext}) and power efficiencies (η_P) as a function of brightness. (e)(f) EL spectra of devices for **CTS** and **CTPS** as a host.

CONCLUSION

In summary, a new type of bended donor-donor-acceptor (DDA) molecule, **CTPS**, is designed and synthesized, which exhibit anomalous excitation-wavelength dependent ratiometric dual emission. With a face-to-face alignment of D1 and A, together with D2 acting as a bridge, this bending type **CTPS** exhibits intramolecular exciplex-like CT(S) emission from D1 to A and intramolecular through-π conjugation CT (CT(B)) from D2 to A in solution, which is a new phenomenon for the D-D-A triad. Further dynamics and theoretical approaches leads us to conclude that CT(B) and CT(S) undergo two independent structural relaxation processes, yielding population branching ratio that is excitation-wavelength dependent. The net result is to exhibit anti-Kasha behavior, rendering a higher state S_2 (CT(B)) emission. Therefore, as for the molecules comprising of multiple donor/acceptor moieties that are current hot topic, one might have to treat it as a molecular composite in which the interplay of CT among the donor/acceptor moieties plays a crucial to account for the unusual photo-physics and/or photochemistry. With prominent TADF emission, the OLEDs with **CTPS** or **CTS** acting as a host have been examined. The external quantum efficiencies of **CTS** hosted (PPy)$_2$Ir(acac) reached 20.4% with extremely low roll-off of efficiency. Thus, with facile tuning of D-D-A type OLED molecules such as the curtailment of one charge transfer distance within **CTS** compared to **CTPS**, higher devices efficiency can be accomplished. This work not only affords an important element that sheds light on the mechanisms of excited-state dynamics of the newly developed bending type D-D-A systems, but also opens new possibilities of selective control of triad OLED molecules via various D1, D2 and acceptor combinations such that a broad range of emission spectrum can be fine-tuned.

ASSOCIATED CONTENT

Supporting Information. Synthetic procedures and characterizations for the new compounds, crystal data, steady and time-resolved spectroscopic data, theoretical calculations, mobility, and device charactristics. The supporting information is available free of charge via the Internet at http://pubs.acs.org.

AUTHOR INFORMATION

Corresponding Author

Wen-Yi Hung: wenhung@mail.ntou.edu.tw;

Ken-Tsung Wong: kenwong@ntu.edu.tw;

Pi-Tai Chou: chop@ntu.edu.tw

Present Addresses

Department of Chemistry, National Taiwan University, Taipei, 10617 Taiwan

Institute of Optoelectronic Sciences, National Taiwan Ocean University, Keelung, 20224, Taiwan

Author Contributions

$^\perp$J.-A. L., S.-W. L. and Z.-Y. L. made equal contributions.

ACKNOWLEDGMENT

ABBREVIATIONS

.

REFERENCES

1.   Chang, C.-H.; Kuo, M.-C.; Lin, W.-C.; Chen, Y.-T.; Wong, K.-T.; Chou, S.-H.; Mondal, E.; Kwong, R. C.; Xia, S.; Nakagawa, T.; Adachi, C., A dicarbazole–triazine hybrid bipolar host material for highly efficient green phosphorescent OLEDs. *J. Mater. Chem.* **2012,** *22*, 3832-3838.

2.   Kim, S. M.; Yun, J. H.; Byeon, S. Y.; Jeon, S. K.; Lee, J. Y., Effect of Interconnection Position of Bicarbazole-Triazine Type Bipolar Host Materials on the Photophysical and Device Performances. *J. Ind. Eng. Chem.* **2017**, *51*, 295-302.

3.   Chatterjee, T.; Hung, W.-Y.; Tang, W.-F.; Chen, H.-F.; Wong, K.-T., Carbazole-Bridged Triphenylamine-Bipyridine Bipolar Hosts for High-Efficiency Low Roll-Off Multi-Color Pholeds. *Org. Electron.* **2017**, *50*, 204-212.

4.   Data, P.; Pander, P.; Okazaki, M.; Takeda, Y.; Minakata, S.; Monkman, A. P., Dibenzo[a,J]Phenazine-Cored Donor–Acceptor–Donor Compounds as Green-to-Red/Nir Thermally Activated Delayed Fluorescence Organic Light Emitters. *Angew. Chem. Int. Ed.* **2016**, *55*, 5739-5744.

5.   Ward, J. S.; Nobuyasu, R. S.; Batsanov, A. S.; Data, P.; Monkman, A. P.; Dias, F. B.; Bryce, M. R., The Interplay of Thermally Activated Delayed Fluorescence (Tadf) and Room Temperature Organic Phosphorescence in Sterically-Constrained Donor–Acceptor Charge-Transfer Molecules. *Chem. Commun.* **2016**, *52*, 2612-2615.

6.   Serevičius, T.; Bučiūnas, T.; Bucevičius, J.; Dodonova, J.; Tumkevičius, S.; Kazlauskas, K.; Juršėnas, S., Room Temperature Phosphorescence Vs. Thermally Activated Delayed Fluorescence in Carbazole–Pyrimidine Cored Compounds. *J. Mater. Chem. C* **2018**, *6*, 11128-11136.

7.   He, X.; Shan, T.; Tang, X.; Gao, Y.; Li, J.; Yang, B.; Lu, P., Highly Efficient Organic Light Emitting Diodes Based on a D–a–D Type Dibenzothiophene Derivative Exhibiting Thermally Activated Delayed Fluorescence with Small Δest. *J. Mater. Chem. C* **2016**, *4*, 10205-10208.

8.   Felouat, A.; D'Aléo, A.; Charaf-Eddin, A.; Jacquemin, D.; Le Guennic, B.; Kim, E.; Lee, K. J.; Woo, J. H.; Ribierre, J.-C.; Wu, J. W.; Fages, F., Tuning the Direction of Intramolecular Charge Transfer and the Nature of the Fluorescent State in a T-Shaped Molecular Dyad. *J. Phys. Chem. A* **2015**, *119*, 6283-6295.

9.   Misra, R.; Chakraborty, P.; Roy, S. C.; Maity, D. K.; Bhattacharyya, S. P., Tailoring of Spectral Response and Intramolecular Charge Transfer in B-Enaminones through Band Gap Tuning: Synthesis, Spectroscopy and Quantum Chemical Studies. *RSC Adv.* **2016**, *6*, 36811-36822.

10.   Younes, A. H.; Zhu, L., Tunable Dual Fluorescence of 3-(2,2′-Bipyridyl)-Substituted Iminocoumarin. *ChemPhysChem* **2012**, *13*, 3827-3835.

11.   Willemse, R. J.; Piet, J. J.; Warman, J. M.; Hartl, F.; Verhoeven, J. W.; Brouwer, A. M., Stepwise Versus Direct Long-Range Charge Separation in Molecular Triads. *J. Am. Chem. Soc.* **2000**, *122*, 3721-3730.

12.   Miyazaki, T.; Shibahara, M.; Fujishige, J.-i.; Watanabe, M.; Goto, K.; Shinmyozu, T., Synthesis and Electronic and Photophysical Properties of [2.2]- and [3.3]Paracyclophane-Based Donor–Donor′–Acceptor Triads. *J. Org. Chem.* **2014**, *79*, 11440-11453.

13.   Lauteslager, Xavier Y.; van Stokkum, Ivo H. M.; van Ramesdonk, H. J.; Bebelaar, D.; Fraanje, J.; Goubitz, K.; Schenk, H.; Brouwer, Albert M.; Verhoeven, Jan W., Conformational Dynamics of Charge-Transfer States in Donor−Bridge−Acceptor Systems. *Eur. J. Org. Chem.* **2001**, *2001*, 3105-3118.

14.   Oosterbaan, Wibren D.; van Gerven, Paul C. M.; van Walree, Cornelis A.; Koeberg, M.; Piet, Jacob J.; Havenith, Remco W. A.; Zwikker, Jan W.; Jenneskens, Leonardus W.; Gleiter, R., Photoinduced Charge Separation in Cyclohexylidene-Based Donor−(Σ-Bridge)−Acceptor Compounds − Building Blocks for Materials. *Eur. J. Org. Chem.* **2003**, *2003*, 3117-3130.

15.   Roquet, S.; Cravino, A.; Leriche, P.; Alévêque, O.; Frère, P.; Roncali, J., Triphenylamine−Thienylenevinylene Hybrid Systems with Internal Charge Transfer as Donor Materials for Heterojunction Solar Cells. *J. Am. Chem. Soc.* **2006**, *128*, 3459-3466.

16.   Kulkarni, A. P.; Kong, X.; Jenekhe, S. A., High-Performance Organic Light-Emitting Diodes Based on Intramolecular Charge-Transfer Emission from Donor–Acceptor Molecules: Significance of Electron- Donor Strength and Molecular Geometry. *Adv. Funct. Mater.* **2006**, *16*, 1057-1066.

17.   Li, W.-J.; Wu, H.-M.; Li, Y.-B.; Hu, C.-P.; Yi, M.-D.; Xie, L.-H.; Chen, L.; Zhao, J.-F.; Zhao, X.-H.; Shi, N.-E.; Qian, Y.; Wang, C.; Wei, W.; Huang, W., Facile synthesis and self-assembly of diazafluorenone-based p–n (donor–acceptor) organic semiconductors. *Tetrahedron* **2012,** *68*, 8216-8221.

18.   Wang, K.; Huang, S.; Zhang, Y.; Zhao, S.; Zhang, H.; Wang, Y., Multicolor Fluorescence and Electroluminescence of an Ict-Type Organic Solid Tuned by Modulating the Accepting Nature of the Central Core. *Chem. Sci.* **2013**, *4*, 3288-3293.

19.   Lee, J.-H.; Shin, H.; Kim, J.-M.; Kim, K.-H. & Kim, J.-J. Exciplex-forming co-host-based red phosphorescent organic light-emitting diodes with long operational stability and high efficiency. *ACS Appl. Mater. Interfaces* **2017**, 9, 3277–3281.

20.   Kim, S.-Y.; Jeong, W.-I.; Mayr, C.; Park, Y.-S.; Kim, K.-H.; Lee, J.-H.; Moon, C.-K.; Brütting, W.; Kim, J.-J., Organic Light-Emitting Diodes with 30% External Quantum Efficiency Based on a Horizontally Oriented Emitter. *Adv. Funct. Mater.* **2013**, 23, 3896 - 3900.

21.   Lee, S.; Kim, K.-H.; Limbach, D.; Park, Y.-S.; Kim, J.-J., Low Roll-Off and High Effi ciency Orange Organic Light Emitting Diodes with Controlled Co-Doping of Green and Red Phosphorescent Dopants in an Exciplex Forming Co-Host. *Adv. Funct. Mater.* **2013**, 23, 4105-4110.

22.   Shin, H.; Lee, S.; Kim, K.-H.; Moon, C.-K.; Yoo, S.-J.; Lee, J.-H.; Kim, J.-J., Blue Phosphorescent Organic Light-Emitting Diodes Using an Exciplex Forming Co-host with the External Quantum Efficiency of Theoretical Limit. *Adv. Mater.* **2014**, 26, 4730-4734.

23.   Sun, J. W.; Lee, J.-H.; Moon, C.-K.; Kim, K.-H.; Shin, H.; Kim, J.-J., A Fluorescent Organic Light-Emitting Diode with 30% External Quantum Effi ciency. *Adv. Mater.* **2014**, 26, 5684-5688.

24.   Park, Y.-S.; Lee, S.; Kim, K.-H.; Kim, S.-Y.; Lee, J.-H.; Kim, J.-J., Exciplex-Forming Co-host for Organic Light-Emitting Diodes with Ultimate Effi ciency. *Adv. Funct. Mater.* **2013**, 23, 4914-1920.

25.   Kabe, R. & Adachi, C. Organic long persistent luminescence. *Nature* **550**, 384 (2017).

26.   Hung, W.-Y.; Fang, G.-C.; Chang, Y.-C.; Kuo, T.-Y.; Chou, P.-T.; Lin, S.-W.; Wong, K.-T., Highly Efficient Bilayer Interface Exciplex For Yellow Organic Light-Emitting Diode. *ACS Appl. Mater. Interfaces* **2013**, 5, 6826-6831.

27.   Lee, J.-H.; Lee, S.; Yoo, S.-J.; Kim, K.-H.; Kim, J.-J., Langevin and Trap-Assisted Recombination in Phosphorescent Organic Light Emitting Diodes. *Adv. Funct. Mater.* **2014**, 24, 4681-4688.

28.   Song, W.; Lee, J. Y., Light emission mechanism of mixed host organic light-emitting diodes. *Appl. Phys. Lett.* **2015**, 106, 123306.

29.   Zhou, D.-Y.; Siboni, H. Z.; Wang, Q.; Liao, L.-S.; Aziz, H., Host to Guest Energy Transfer Mechanism in Phosphorescent and Fluorescent Organic Light-Emitting Devices Utilizing Exciplex-Forming Hosts. *J. Phys. Chem. C* **2014**, 118, 24006-24012.

30.   Yu, W.-S.; Cheng, C.-C.; Cheng, Y.-M.; Wu, P.-C.; Song, Y.-H.; Chi, Y.; Chou, P.-T., Excited-State Intramolecular Proton Transfer in Five-Membered Hydrogen-Bonding Systems: 2-Pyridyl Pyrazoles. *J. Am. Chem. Soc.* **2003**, *125*, 10800-10801.

31.   Yushchenko, D. A.; Shvadchak, V. V.; Klymchenko, A. S.; Duportail, G.; Mély, Y.; Pivovarenko, V. G., 2-Aryl-3-Hydroxyquinolones, a New Class of Dyes with Solvent Dependent Dual Emission Due to Excited State Intramolecular Proton Transfer. *New J. Chem.* **2006**, *30*, 774-781.

32.   Suzuki, N.; Fukazawa, A.; Nagura, K.; Saito, S.; Kitoh-Nishioka, H.; Yokogawa, D.; Irle, S.; Yamaguchi, S., A Strap Strategy for Construction of an Excited-State Intramolecular Proton Transfer (Esipt) System with Dual Fluorescence. *Angew. Chem. Int. Ed.* **2014**, *53*, 8231-8235.

33.   Li, W.; Liu, D.; Shen, F.; Ma, D.; Wang, Z.; Feng, T.; Xu, Y.; Yang, B.; Ma, Y., A Twisting Donor-Acceptor Molecule with an Intercrossed Excited State for Highly Efficient, Deep-Blue Electroluminescence. *Adv. Funct. Mater.* **2012**, *22*, 2797-2803.

34.   Thiagarajan, V.; Selvaraju, C.; Malar, E. J. P.; Ramamurthy, P., A Novel Fluorophore with Dual Fluorescence: Local Excited State and Photoinduced Electron-Transfer-Promoted Charge-Transfer State. *ChemPhysChem* **2004**, *5*, 1200-1209.

35.   Nobuyasu, R. S.; Ren, Z.; Griffiths, G. C.; Batsanov, A. S.; Data, P.; Yan, S.; Monkman, A. P.; Bryce, M. R.; Dias, F. B., Rational Design of Tadf Polymers Using a Donor–Acceptor Monomer with Enhanced Tadf Efficiency Induced by the Energy Alignment of Charge Transfer and Local Triplet Excited States. *Adv. Opt. Mater.* **2016**, *4*, 597-607.

36.   Dias, F. B.; Santos, J.; Graves, D. R.; Data, P.; Nobuyasu, R. S.; Fox, M. A.; Batsanov, A. S.; Palmeira, T.; Berberan-Santos, M. N.; Bryce, M. R.; Monkman, A. P., The Role of Local Triplet Excited States and D-a Relative

Orientation in Thermally Activated Delayed Fluorescence: Photophysics and Devices. *Adv. Sci.* **2016**, *3*, 1600080.

37.   Yao, L.; Pan, Y.; Tang, X.; Bai, Q.; Shen, F.; Li, F.; Lu, P.; Yang, B.; Ma, Y., Tailoring Excited-State Properties and Electroluminescence Performance of Donor–Acceptor Molecules through Tuning the Energy Level of the Charge-Transfer State. *J. Phys. Chem. C* **2015**, *119*, 17800-17808.

38.   Liu, B.; Wang, J.; Zhang, G.; Bai, R.; Pang, Y., Flavone-Based Esipt Ratiometric Chemodosimeter for Detection of Cysteine in Living Cells. *ACS Appl. Mater. Interfaces* **2014**, *6*, 4402-4407.

39.   Liu, B.; Wang, H.; Wang, T.; Bao, Y.; Du, F.; Tian, J.; Li, Q.; Bai, R., A New Ratiometric Esipt Sensor for Detection of Palladium Species in Aqueous Solution. *Chem. Commun.* **2012**, *48*, 2867-2869.

40.   Tang, K.-C.; Chang, M.-J.; Lin, T.-Y.; Pan, H.-A.; Fang, T.-C.; Chen, K.-Y.; Hung, W.-Y.; Hsu, Y.-H.; Chou, P.-T., Fine Tuning the Energetics of Excited-State Intramolecular Proton Transfer (Esipt): White Light Generation in a Single Esipt System. *J. Am. Chem. Soc.* **2011**, *133*, 17738-17745.

41.   Tseng, H.-W.; Liu, J.-Q.; Chen, Y.-A.; Chao, C.-M.; Liu, K.-M.; Chen, C.-L.; Lin, T.-C.; Hung, C.-H.; Chou, Y.-L.; Lin, T.-C.; Wang, T.-L.; Chou, P.-T., Harnessing Excited-State Intramolecular Proton-Transfer Reaction Via a Series of Amino-Type Hydrogen-Bonding Molecules. *J. Phys. Chem. Lett.* **2015**, *6*, 1477-1486.

42.   Demchenko, A. P.; Tang, K.-C.; Chou, P.-T., Excited-State Proton Coupled Charge Transfer Modulated by Molecular Structure and Media Polarization. *Chem. Soc. Rev.* **2013**, *42*, 1379-1408.

43.   Serdiuk, I. E., White Light from a Single Fluorophore: A Strategy Utilizing Excited-State Intramolecular Proton-Transfer Phenomenon and Its Verification. *J. Phys. Chem. C* **2017**, 121, 5277-5286.

44.   Park, S.; Kwon, J. E.; Kim, S. H.; Seo, J.; Chung, K.; Park, S.-Y.; Jang, D.-J.; Medina, B. M.; Gierschner, J.; Park, S. Y., A White-Light-Emitting Molecule: Frustrated Energy Transfer between Constituent Emitting Centers. *J. Am. Chem. Soc.* **2009**, 131, 14043-14049.

45.   Skonieczny, K.; Yoo, J.; Larsen, J. M.; Espinoza, E. M.; Barbasiewicz, M.; Vullev, V. I.; Lee, C.-H.; Gryko, D. T., How To Reach Intense Luminescence for Compounds Capable of Excited-State Intramolecular Proton Transfer? *Chem. Eur. J.* **2016**, 22, 7485-7496.

46.   Moore, T. A.; Gust, D.; Mathis, P.; Mialocq, J.-C.; Chachaty, C.; Bensasson, R. V.; Land, E. J.; Doizi, D.; Liddell, P. A.; Lehman, W. R.; Nemeth, G. A.; Moore, A. L., Photodriven charge separation in a carotenoporphyrin–quinone triad. *Nature* **1984**, 307, 630-632.

47.   Liddell, P. A.; Kuciauskas, D.; Sumida, J. P.; Nash, B.; Nguyen, D.; Moore, A. L.; Moore, T. A.; Gust, D., Photoinduced Charge Separation and Charge Recombination to a Triplet State in a Carotene−Porphyrin−Fullerene Triad. *J. Am. Chem. Soc.* **1997**, 119, 1400-1405.

48.   Chen, D.-G.; Lin, T.-C.; Chen, Y.-A.; Chen, Y.-H.; Lin, T.-C.; Chen, Y.-T.; Chou, P.-T., Revisiting Dual Intramolecular Charge-Transfer Fluorescence of Phenothiazine-Triphenyltriazine Derivatives. *J. Phys. Chem. C* **2018**, *122*, 12215-12221.

49.   Demchenko, A. P.; Tomin, V. I.; Chou, P.-T., Breaking the Kasha Rule for More Efficient Photochemistry. *Chem. Rev.* **2017**, *117*, 13353-13381.

50.   Haidekker, M. A.; Brady, T. P.; Lichlyter, D.; Theodorakis, E. A., Effects of solvent polarity and solvent viscosity on the fluorescent properties of molecular rotors and related probes. *Bioorg. Chem.* **2005,** *33*, 415-425.

51.   Druzhinin, S. I.; Ernsting, N. P.; Kovalenko, S. A.; Lustres, L. P.; Senyushkina, T. A.; Zachariasse, K. A., Dynamics of Ultrafast Intramolecular Charge Transfer with 4-(Dimethylamino)benzonitrile in Acetonitrile. *J. Phys. Chem. A* **2006,** *110*, 2955-2969.

52.   Chen, D.-G.; Lin, T.-C.; Chen, C.-L.; Chen, Y.-T.; Chen, Y.-A.; Lee, G.-H.; Chou, P.-T.; Liao, C.-W.; Chiu, P.-C.; Chang, C.-H.; Lien, Y.-J.; Chi, Y., Optically Triggered Planarization of Boryl-Substituted Phenoxazine: Another Horizon of Tadf Molecules and High-Performance Oleds. *ACS Appl. Mater. Interfaces* **2018**, *10*, 12886-12896.

53.   Tsai, W.-L.; Huang, M.-H.; Lee, W.-K.; Hsu, Y.-J.; Pan, K.-C.; Huang, Y.-H.; Ting, H.-C.; Sarma, M.; Ho, Y.-Y.; Hu, H.-C.; Chen, C.-C.; Lee, M.-T.; Wong, K.-T.; Wu, C.-C., A versatile thermally activated delayed fluorescence emitter for both highly efficient doped and non-doped organic light emitting devices. *Chemical Communications* **2015,** *51*, 13662-13665.

54.   Lin, M.-S.; Yang, S.-J.; Chang, H.-W.; Huang, Y.-H.; Tsai, Y.-T.; Wu, C.-C.; Chou, S.-H.; Mondal, E.; Wong, K.-T., Incorporation of a CN group into mCP: a new bipolar host material for highly efficient blue and white electrophosphorescent devices. *J. Mater. Chem.*, **2012**, *22*, 16114.

55.   Adachi, C.; Baldo, M. A.; Thompson, M. E.; Forrest, S. R., Nearly 100% internal phosphorescence efficiency in an organic light-emitting device. *J. Appl. Phys.* **2001**, *90*, 5048.

56.   Lamansky, S.; Djurovich, P.; Murphy, D.; Abdel-Razzaq, F.; Lee, H.-E.; Adachi, C.; Burrows, P. E.; Forrest, S. R.; Thompson, M. E., Highly Phosphorescent Bis-Cyclometalated Iridium Complexes: Synthesis, Photophysical Characterization, and Use in Organic Light Emitting Diodes. *J. Am. Chem. Soc.* **2001**, *123*, 4304.

57.   Endo, A.; Adachi, C., Photoluminescence characteristics of tris(2-phenylquinoline)iridium(III) dispersed in an iridium complex host layer. *Chem. Phys. Lett.* **2009**, *483*, 224.

58.   Hung, W.-Y.; Tsai, T.-C.; Su, S.-Y.; Wong, K.-T.; Chi, L.-C., An ambipolar host material provides highly efficient saturated red PhOLEDs possessing simple device structures. *Phys. Chem. Chem. Phys.* **2008**, *10*, 5822.

59.   Leem, D.-S.; Park, H.-D.; Kang, J.-W.; Lee, J.-H.; Kim, J. W.; Kim, J.-J., Low driving voltage and high stability organic light-emitting diodes with rhenium oxide-doped hole transporting layer. *Appl. Phys. Lett.* **2007**, *91*, 011113.

60.   Yoo, S.-J.; Chang, J.-H.; Lee, J.-H.; Moon, C.-K.; Wu, C.-I.; Kim, J.-J., Formation of perfect ohmic contact at indium tin oxide/N,N'-di(naphthalene-1-yl)-N,N'-diphenyl-benzidine interface using ReO$_3$. *Sci. Rep.* **2014**, *4*, 3902.

61.   Ma, X.; Liang, J.; Bai, F.; Ye, K.; Xu, J.; Zhu, D.; Bryce, M. R., New Mixed-C^N Ligand Tris-Cyclometalated Ir^{III} Complexes for Highly-Efficient Green Organic Light-

Emitting Diodes with Low Efficiency Roll-Off. *Eur. J. Inorg. Chem.* **2018**, 4614-4621.

1
2
3
4
5
6
7
8
9
10
11
12
13
14
15
16
17
18
19
20
21
22
23
24
25
26
27
28
29
30
31
32
33
34
35
36
37
38
39
40
41
42
43
44
45
46
47
48
49
50
51
52
53
54
55
56
57
58
59
60

Table of Content Graphic:

D1-D2-A
Molecular
Triad

Through Bond CT
Classic Fluorescence

Through Space CT
TADF Character

Anti Kasha Excitation-Wavelength Dependent Emissions